Dynamic development of the calyx of Held synapse

Adrián Rodríguez-Contreras*, John Silvio Soria van Hoeve, Ron L. P. Habets†, Heiko Locher, and J. Gerard G. Borst

Department of Neuroscience, Erasmus MC, University Medical Center Rotterdam, Dr. Molewaterplein 50, 3015 GE Rotterdam, The Netherlands

Communicated by Erwin Neher, Max Planck Institute for Biophysical Chemistry, Göttingen, Germany, February 12, 2008 (received for review January 11, 2008)

The calyx of Held is probably the largest synaptic terminal in the brain, forming a unique one-to-one connection in the auditory ventral brainstem. During early development, calyces have many collaterals, whose function is unknown. Using electrophysiological recordings and fast-calcium imaging in brain slices, we demonstrate that these collaterals are involved in synaptic transmission. We show evidence that the collaterals are pruned and that the pruning already begins 1 week before the onset of hearing. Using two-photon microscopy to image the calyx of Held in neonate rats, we report evidence that both axons and nascent calyces are structurally dynamic, showing the formation, elimination, extension, or retraction of up to 65% of their collaterals within 1 hour. The observed dynamic behavior of axons may add flexibility in the choice of postsynaptic partners and thereby contribute to ensuring that each principal cell eventually is contacted by a single calyx of Held.

auditory system | medial nucleus of the trapezoid body | two-photon imaging | structural plasticity | axon collateral

Studying the formation of individual, identified synapses in the CNS presents a formidable challenge because of their small size, their incredibly high density, and their protracted formation period (1). Imaging studies in living animals have provided insights into the structural changes that presynaptic axons undergo during development, which complements our understanding of how specific brain connections form (2). An emerging view from these studies is that axonal dynamics are age- and cell type-dependent (3) and strongly correlated with the formation of synaptic contacts, which may ultimately guide the growth of the axonal arbor (2, 4–6).

Here, we study the development of a CNS synapse that can be identified relatively easily because it is probably the largest synaptic contact in the mammalian brain (7). The calyx of Held connects the globular bushy cells of the anteroventral cochlear nucleus and the principal cells of the medial nucleus of the trapezoid body (MNTB) in the brainstem. Studies in rodents have shown that shortly before birth, the principal cells of the MNTB are innervated by small glutamatergic boutons (8). Morphological and functional identification of nascent calyces is possible between postnatal days 3 and 5 (8–10), which suggests that the characteristic one-to-one innervation observed in mature animals is achieved very rapidly (10). However, previous studies have not been able to study the dynamic aspects of the calyx of Held development.

As a first step toward elucidating the cellular mechanisms that ensure that each MNTB principal cell is always innervated by only a single calyx of Held, we sought an imaging approach. Because it has not been possible to study this unique synapse in culture, we carried out studies *in vivo*. We developed a surgical procedure to label brainstem axons in anesthetized rat pups and imaged them with a two-photon microscope. Using this approach, we provide evidence of structural dynamics related to the development of the calyx of Held synapse. In combination with electrophysiological and optical recordings in brain slices, neuronal tracing, and immunohistochemistry we show that single axons in the MNTB can innervate multiple postsynaptic cells through the collaterals of the calyx of Held.

Results

Relation Between Large Axosomatic Contacts and Synaptic Clusters. Brainstem sections containing the MNTB at different postnatal ages were stained immunohistochemically for VGLUT, a presynaptic marker of excitatory synapses, and analyzed by using fluorescence microscopy (Fig. 1). At postnatal day 2 (P2) and younger ages, punctate labeling was observed both in the neuropil and around cell bodies in the MNTB. At P3 and beyond, large perisomatic presynaptic clusters (LPCs) of VGLUT staining were present (Fig. 1 *A* and *B*). The fraction of cells surrounded by LPCs increased with age. In the medial part of the MNTB, the increase was more rapid than in the lateral part (*t* test, $P < 0.001$; two animals per age and at least two images per animal; Fig. 1*C*). We examined the relationship between the synaptic marker staining and axonal morphology by prelabeling the axons with a fluorescent tracer. At P3, large axosomatic contacts were observed, which stained positive for VGLUT, but only 30% of these contacts showed an LPC (Fig. 1*B*, compare *Left* and *Center*, and *D*). In control P8 sections, the majority of large terminals could be associated with an LPC (Fig. 1*B*, *Right*, and *D*). Therefore, it is unlikely that the fluorescent tracer interfered with the immunohistochemical marking of the presynaptic clusters at P3. Next, we used image segmentation and colocalization procedures to estimate the density and size of VGLUT clusters within labeled axons [see supporting information (SI) *Materials and Methods*]. This analysis showed only modest differences between axons at ages P1 and P3 (Fig. 1 *E* and *F*). In contrast, the relative volume of VGLUT clusters associated with large axosomatic contacts at P3 was clearly larger (Fig. 1*F*). Overall, these results suggest that most large axosomatic contacts take at most 1 day to form but that the packing of these early calyces with synaptic glutamatergic vesicles generally takes several days.

Measurement of Synaptic Responses in Principal Cells During the Period of Calyx Formation. Examination of labeled tissue at P3 showed the presence of relatively small presynaptic clusters outside the large axosomatic contact area (Fig. 1*B*, *Center*), suggesting that synaptic terminals from nonlabeled axons were also contacting these postsynaptic cells. Therefore, we examined the possibility that principal cells receive synaptic inputs from multiple axons at ages P2–3. We made whole-cell recordings of principal cells in slices in which trapezoidal axons were prelabeled with a fluorescent tracer (see Fig. S1). In these experiments, excitatory postsynaptic currents (EPSCs) were evoked by electrical stimulation at the midline. Despite the prominent

Author contributions: A.R.-C. and J.G.G.B. designed research; A.R.-C., J.S.S.v.H., R.L.P.H., H.L., and J.G.G.B. performed research; A.R.-C., J.S.S.v.H., R.L.P.H., H.L., and J.G.G.B. analyzed data; and A.R.-C. and J.G.G.B. wrote the paper.

The authors declare no conflict of interest.

*To whom correspondence should be addressed. E-mail: a.rodriguezcontreras@erasmusmc.nl.

†Present address: Laboratory of Neuronal Communication, Molecular and Developmental Genetics, Department of Human Genetics, University of Leuven, Herestraat 49, 3000 Leuven, Belgium.

This article contains supporting information online at www.pnas.org/cgi/content/full/0801395105/DCSupplemental.

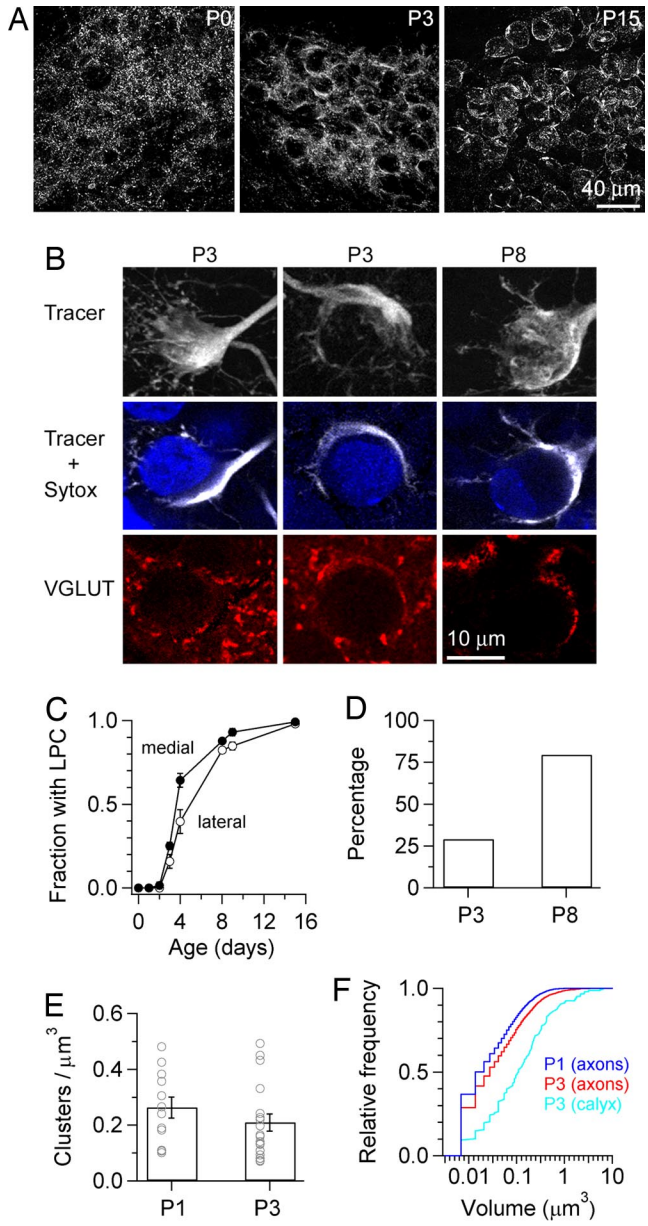

Fig. 1. Presynaptic clusters during postnatal development. (*A*) Confocal z-stack projections show the distribution of VGLUT label in the medial half of the MNTB at P0, P3, and P15. Lateral is right, dorsal is up. (*B*) Perisomatic labeling of VGLUT-positive clusters is revealed in triple-stained tissue. (*Top*) Z-stack projection of calyces that were labeled with a fluorescent dextran (gray scale). (*Middle* and *Bottom*) Single confocal sections from the same focal plane demonstrating the location of the postsynaptic cell (counterstained with SYTOX, color-coded blue) and the presynaptic clusters (color-coded red), respectively. (*C*) The fraction of perisomatic LPCs in medial and lateral regions of the MNTB increased during postnatal development. (*D*) Percentage of large axosomatic contacts that were colabeled with an LPC at P3 (31 contacts from three animals) and in control sections at P8 (29 contacts from one animal). (*E*) Density of presynaptic clusters in labeled axons at P1 and P3. (*F*) Cumulative histogram of presynaptic cluster volume for axons at P1 and P3 (blue and red, respectively) and for calyces of Held at P3 (cyan; 31 labeled axons). Confocal images were contrasted with Adobe Photoshop.

presence of delayed release (11), it was clear that the average amplitude increased with increasing stimulus intensity ($n = 10$ of a total of 10 cells; Fig. 2). Together with our histological analysis (see Fig. S1), the data are consistent with the recruitment of multiple axons with distinct activation thresholds. We conclude

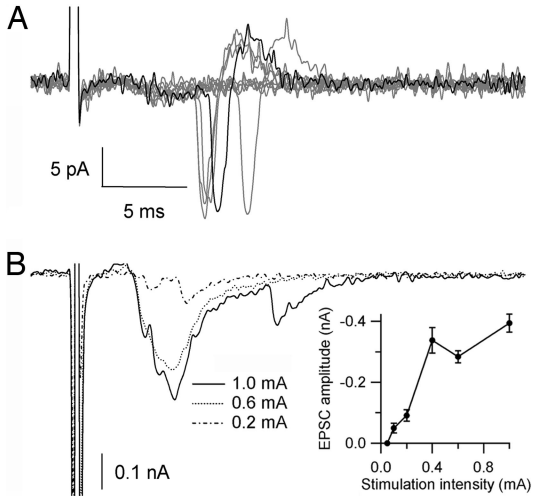

Fig. 2. Multiple glutamatergic inputs to MNTB cells in neonate rats. (*A*) Cell-attached recordings show action potential currents at 1-mA stimulation. (*B*) Whole-cell voltage-clamp recordings show the responses of the MNTB cell to different stimulation intensities (dashed-punctate, punctate, or continuous lines). (*Inset*) Input–output curve shows a graded increase in the amplitude of the EPSC with increasing stimulation intensity (mean ± SEM, 10 traces per stimulus intensity). Note that EPSC amplitude is displayed as a vertical increase, and the negative sign indicates the inward current.

that during early postnatal development, MNTB cells receive small-amplitude glutamatergic contacts from multiple axons.

***In Vivo* Imaging of Axons and Synaptic Terminals in the MNTB of Neonate Rats.** We used two-photon microscopy to image axons that had been prelabeled by injecting a fluorescent tracer in anesthetized rat pups (Fig. 3). In these acute experiments, we were able to visualize several individual axons, confirming the presence of calyx-like structures at P3 (Fig. 3 *A* and *B*). Retro-

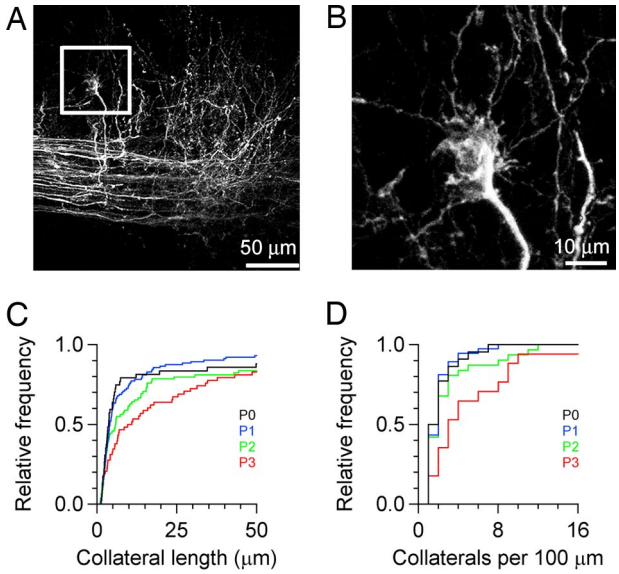

Fig. 3. *In vivo* two-photon imaging in the MNTB of neonate rats. (*A*) Exemplar image of labeled axons at P3. (*Inset*) Location of a calyx of Held terminal. (*B*) Close-up view of the labeled calyx in *A*. (*C*) Axon collateral length was traced in at least three z-stacks from different animals and plotted as a cumulative histogram. (*D*) Cumulative histogram of the number of collaterals per 100 μm of axon. Two-photon images are collapsed z-stacks of >50 optical slices acquired at 1-μm intervals.

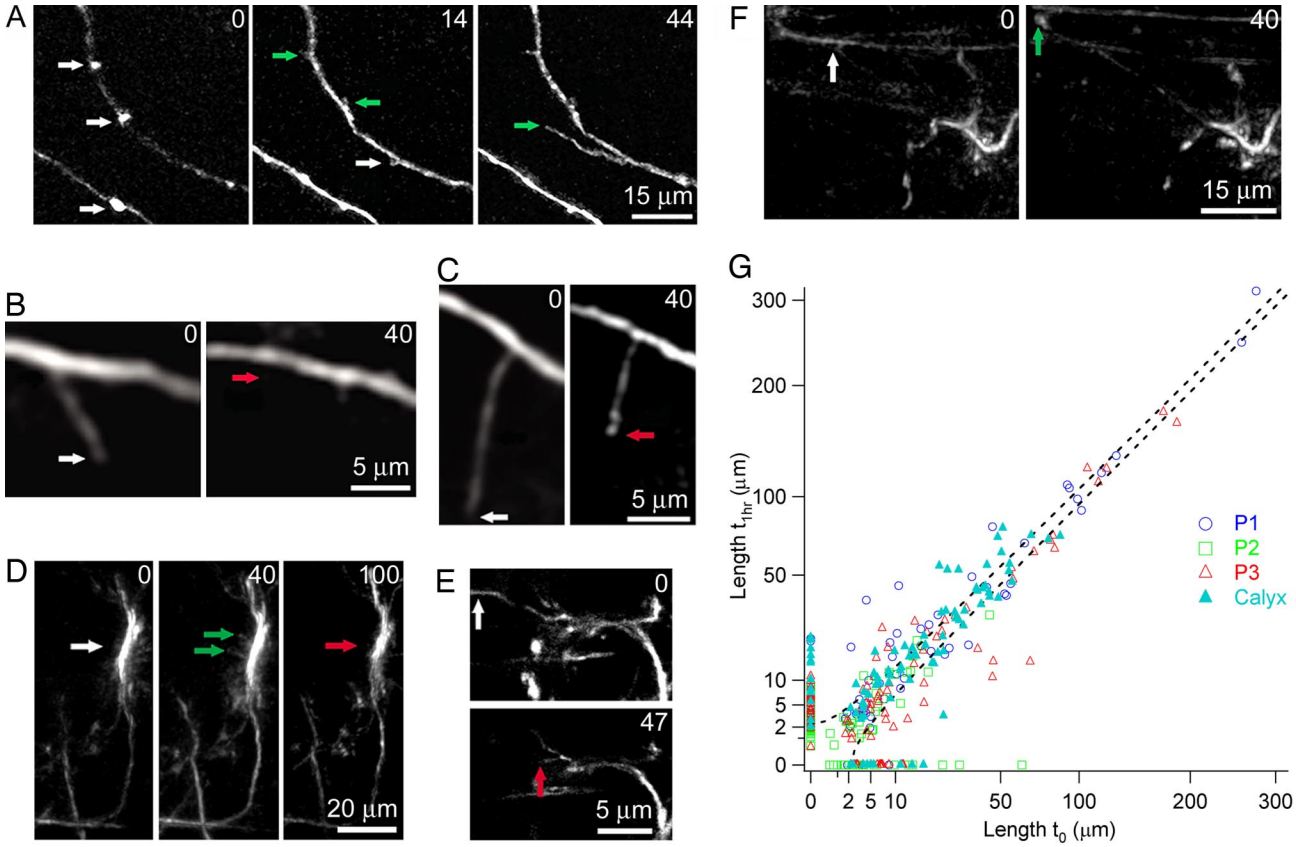

Fig. 4. Turnover and motility of axon and calyx of Held collaterals. Time lapse images were acquired at ages P1–3. (*A*) Sequence of images obtained at different time points shows three swellings on two labeled axons at P1 (*Left*, white arrows). One axon formed three short protrusions (*Center*, two formed near swellings, green arrows, and one formed from the shaft of the axon, white arrow). Two of the small protrusions did not change, whereas the third one increased in length (*Right*, green arrow). The second axon did not add branches within this time period, but some changes in the identified swelling were noticed. (*B*) Short axon collateral at P2 (*Left*, white arrow). In this case, the collateral could not be located anymore after 40 min, indicating that it was lost (*Right*, red arrow). (*C*) Image sequence of an axon collateral at P2 (*Left*, white arrow) shows the retraction of the collateral tip (*Right*, red arrow). (*D*) Time lapse imaging revealed the formation (*Center*, green arrows) and loss (*Right*, red arrow) of calyx of Held collaterals. (*E*) Retraction of a calyx of Held collateral (*Lower*, red arrow). (*F*) Calyx of Held collateral (*Left*, white arrow) extended after 40 min (*Right*, red arrow). (*G*) Plot of the initial collateral length vs. the corresponding length 1 h later. Data are compared between collaterals of the calyx of Held at P3 vs. axons at ages P1–3 as indicated by different colors and symbols. Images are collapsed stacks of at least three optical slices acquired at 1-μm intervals. Dashed black lines in *G* indicate the confidence interval for assigning a change in length (see *SI Materials and Methods*). (*A–F*) Numbers on the *Top Right* or *Left* corners indicate the time in minutes.

spective analysis confirmed that these structures were large axosomatic contacts located in the MNTB (see Fig. S2). Next, we reconstructed the trajectory of >100 axons in two-photon image stacks and measured the length and density of all visible extensions per axon (total measured axon length, 30 mm; average axon segment, 200 ± 10 μm, $n = 12$ rats). Cumulative histogram analysis of the length and number of axonal extensions suggested that during the 1st days of postnatal life, axons grow both by adding and by extending collaterals (Fig. 3 *C* and *D*).

To study the dynamics of axon collateral growth, we carried out time lapse experiments in different animals between ages P1 and P3. A striking feature of the data was the dynamics of the axons. Whereas the average increase in the length of the collaterals between P0 and P3 was <10 μm per day, only approximately one-third of the axons were stable within the observation period of 1 h. Some collaterals formed from axonal shafts by interstitial growth (3), whereas others extended, retracted or disappeared, within a time frame of minutes (Fig. 4 *A–C*). To quantify and compare the structural changes in a larger sample of imaged axons across different ages, we plotted the initial length of a total of 301 individual axon collaterals against their corresponding length 1 h later (Fig. 4*G*). Using conservative criteria to score for changes in collateral length (see *SI Materials and Methods*), we identified five categories of axon collaterals: stable, added, lost, extended, and retracted (4).

The dynamics of the axons were age-dependent. P1 appears to be a period of expansion, with 21% of axons added and 24% extended, and only 3% lost and 14% retracted (see Table S1). At P2 and P3, close before and during the formation of calyx-type synapses, a large fraction of collaterals were either added or lost (P2: 24% added, 32% lost; P3: 25% added, 15% lost), with fewer collaterals changing their length (P2: 7% extended, 8% retracted; P3: 10% extended, 20% retracted). The calyx of Held collaterals were also dynamic at P3 (Fig. 4 *D–F*). Although the percentage of calyx collaterals that were added or lost within the 1-h observation period was smaller than of axon collaterals at the same age (14% added, 11% lost), the fraction of collaterals changing their length was similar to the situation at P1 (26% extended, 15% retracted).

The average length of the collaterals that formed or disappeared was typically much smaller than the collaterals that were in the stable, extended, or retracted category, except for P2, where relatively short collaterals were observed (see Table S2). In summary, these data show that axon and calyx of Held collaterals form interstitially and that a majority of the collaterals exhibit different levels of turnover (addition and loss) and motility (extension and

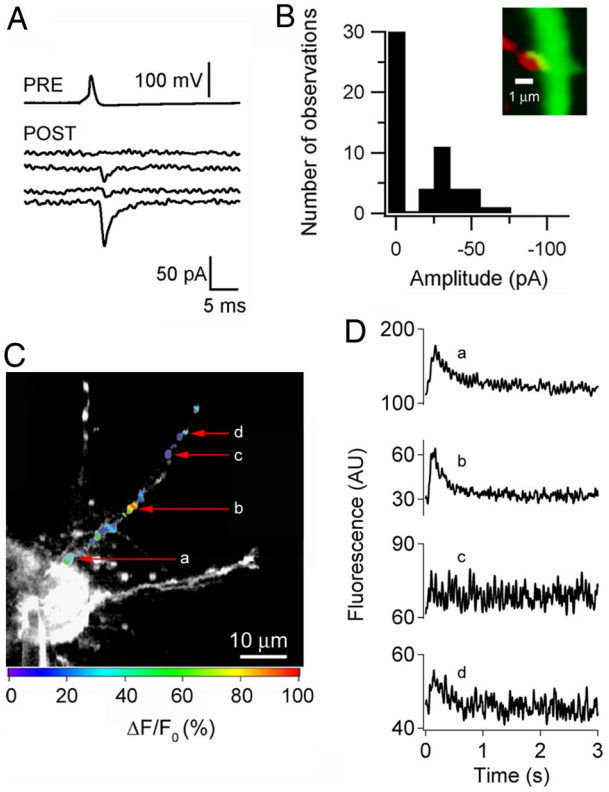

Fig. 5. Calyx of Held collaterals can form functional synapses on adjacent principal cells. Paired recordings between a calyx of Held and a nearby principal cell were performed in acute slices at P4. (*A*) Presynaptic action potentials were triggered in current clamp mode in the calyx (PRE) by injecting 0.3 nA for 2 ms at 0.2 Hz, whereas EPSCs were measured in voltage clamp in the postsynaptic cell (POST). After presynaptic action potentials, a failure, two small responses, and a larger response were observed in the postsynaptic recording. Postsynaptic traces have been vertically offset for display purposes. (*B*) Amplitude distribution of EPSCs. Note the presence of failures after >50% of the stimulations. Bin size is 10 pA. (*Inset*) Contact region between the calyx of Held collateral (red) and a spine-like structure on the dendrite of the postsynaptic MNTB cell (green). Note the inverted horizontal axis, with larger EPSCs being more negative. (*C*) Localized AP-evoked calcium transients in a calyx of Held collateral filled with OGB-1 using a patch pipette. The color code for the spatial distribution of the peak $\Delta F/F_0$ fluorescence is shown on the *Bottom*. (*D*) Representative calcium transients recorded during rapid line scanning at locations *a–d* indicated in *C*.

retraction) across ages. Based on the observed structural dynamics in the calyx of Held terminal, we wondered whether the collaterals of the calyx of Held could have an involvement in synaptic function during postnatal development.

Functional Analysis of Calyx of Held Collaterals. To test whether calyx of Held collaterals make functional synaptic contacts, we carried out paired patch clamp recordings in brain slices between a presynaptic terminal and an off-target MNTB cell. Presynaptic action potentials triggered small, short-latency EPSCs (Fig. 5 *A* and *B*). In these experiments, we were able to confirm a morphological apposition between the calyx of Held collateral and the dendrite of the postsynaptic cell ($n = 3$ connected pairs of 11 paired recordings at P4; Fig. 5*B*, *Inset*). In two experiments, the slice was fixed, resectioned, and processed for VGLUT immunohistochemistry. Doing so confirmed the presence of an LPC in the recorded terminal and demonstrated that smaller, punctate presynaptic clusters can originate from calyx of Held collaterals (see Fig. S3). Interestingly, the MNTB cells did not generally show an LPC in connected pairs, although examples of cells with an LPC were observed in nonconnected pairs.

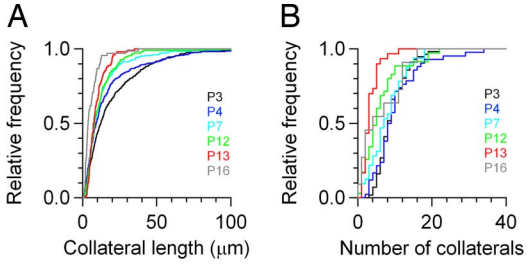

Fig. 6. Calyx of Held collaterals are pruned during postnatal development. Axons were labeled in brain slices, fixed, and imaged with a confocal microscope. The length and number of collaterals were traced at different ages. (*A*) Cumulative histogram of collateral length shows a gradual decrease in collateral length between P3 and P16. (*B*) Cumulative histogram of the number of branches per calyx shows abrupt changes between P13 and P16.

To determine whether MNTB cells with a calyceal input also received smaller inputs, possibly from collaterals of another calyx of Held, we tested the response of principal cells to afferent stimulation in slices at P4. These experiments indicated that MNTB cells with a large input also received short-latency, smaller-amplitude inputs (see Fig. S4).

Finally, we carried out experiments in which we loaded calyx terminals with the calcium dye Oregon green BAPTA-1. We then triggered a sequence of four action potentials at 100 Hz by current injection via the patch pipette while measuring fluorescence by rapidly scanning along a line through both calyx and its collaterals. Action potential-evoked calcium transients were observed in 31 of a total of 41 collaterals from 14 calyces (seven animals, ranging from P5 to P8). Calcium transient amplitudes in collaterals ranged from 15 to 100% $\Delta F/F_0$ and were generally somewhat smaller than the calcium transient evoked simultaneously in the calyx, where the average response ranged from 25 to 125% $\Delta F/F_0$. In some cases, collateral transients were localized to thickenings (Fig. 5 *C* and *D*). Interestingly, although their time course generally matched the time course of the calcium transients evoked simultaneously in the calyx, both the time course and the amplitudes of the calcium transients varied considerably, not only within a single collateral (Fig. 5*D*) but also within one calyx (data not shown). We conclude that many calyx of Held collaterals can make functional contacts with off-target principal cells and that voltage-dependent local increases in calcium are available to support chemical transmission in these structures.

Time Course of Pruning of the Calyx of Held Collaterals. The calyx of Held undergoes a dramatic functional and structural transformation between the 2nd and 3rd postnatal weeks (9, 12, 13). To evaluate the stereotypical pruning of the calyx of Held collaterals, we injected fluorescent tracers in brain slices to label axons in the MNTB between postnatal ages P3 and P16. We then imaged labeled calyces and traced the collaterals to determine the age-dependent changes in length and number of collaterals. Both collateral length and number decreased with age (Fig. 6). Collateral length showed a gradual decrease, whereas collateral number showed more abrupt changes between P12 and 13 and between P13 and 16. These data show that a decrease in collateral length already begins at P4, 1 week before the onset of hearing, which in the rat takes place ≈P10–12 (14) but continues afterward. Based on the electrophysiological, optical, and morphological data, we conclude that pruning of the calyx of Held collaterals results in the elimination of synapses in the MNTB.

Discussion

In this work, we show that it is possible to perform *in vivo* two-photon imaging of developing axons in the mammalian

brainstem. In combination with immunohistochemistry and cell physiology, we show evidence that the development of the calyx of Held synapse consists of two stages. In the first 3 postnatal days, a surprisingly high level of collateral dynamics in both axons and nascent synaptic terminals was observed, and principal cells received synaptic inputs from multiple axons. During this period, formation of a calyx synapse took place on the majority of principal cells at P3. In the second phase, which continued at least until the onset of hearing, large presynaptic clusters of VGLUT-positive vesicles appeared, and the calyx of Held collaterals gradually disappeared, although we showed that during this period collaterals of nascent calyces were able to sustain synaptic transmission with other MNTB cells.

Comparison with Previous Studies. We find that the calyx of Held largely forms around P3 but that there is a much slower phase of refinement during which the calyceal collaterals gradually disappear. To the extent that a comparison is possible, this time course matches earlier experiments performed in rat, cat, mouse, or gerbil (8–10, 15), suggesting that the development of this synapse is highly conserved across species. The essential steps are happening largely before the onset of hearing, supporting the view that sensory activity does not play a major role in the formation of this synapse (10, 16, 17). The formation of the large presynaptic clusters of glutamatergic vesicles was also surprisingly slow. Although we did not directly correlate these stainings with synaptic transmission, our data suggest that one should be cautious in using the amplitude of postsynaptic currents to identify calyceal inputs (10, 18, 19), without additional criteria such as immunohistochemistry or the presence of a prespike.

Origin and Functional Properties of the Calyceal Collaterals. The calyceal collaterals were already identified in the first Golgi studies (20), but it was unknown what their functional significance was and whether they formed before or after the calyx. We present evidence from immunohistochemistry, calcium imaging, and electrophysiology that the calyceal collaterals can innervate adjacent principal cells. Using *in vivo* two-photon imaging, we could directly observe the addition of new calyceal collaterals. The emergence of collaterals from the calyx of Held is in agreement with what has been observed at the frog neuromuscular junction, where differentiated presynaptic sites are hot spots for the emergence of new branches (4). Interestingly, the turnover of calyx of Held collaterals showed a balance between additions and losses that was not present in axon collaterals at the same age. Studies in cultured neurons (21, 22) and in living animals (5, 6, 23, 24) have shown a link between branch dynamics and the presence and strength of synaptic terminals. Therefore, it is tempting to speculate that the calyx of Held could stabilize the axonal arbor. We obtained indirect evidence that some calyceal collaterals formed already before the calyx. We showed that MNTB principal cells receive multiple inputs at P2–3 and that principal cells receive small- and large-amplitude inputs at P4. The small inputs differed from the noncalyceal inputs described (10, 25, 26) because their threshold differed only slightly from the larger inputs and they typically had short latency and fast rise times. A parsimonious interpretation of these findings is that some calyx of Held collaterals are remnants of the initially divergent innervation of principal cells by afferent axons.

How Does Each Principal Cell End Up with a Single Calyx of Held? We observed that the postnatal axons that ultimately form the calyx of Held are very dynamic, suggesting that they are actively exploring the local environment. With the 1-h sampling period, we may have even underestimated the dynamics (27). It is tempting to speculate that the dynamic behavior of these axons and synaptic terminals increases the number of principal cells that are contacted by each axon and thereby increases the flexibility and reliability of the mechanism that ensures the one-to-one innervation of this auditory pathway. The mechanisms that favor the formation of a calyx of Held from its axonal precursors are independent of sensory function. They deserve further study, and we expect that the *in vivo* imaging approach that we present here will help toward the further elucidation of the different steps involved in the formation of this synapse.

Materials and Methods

Rats. Wistar rats were purchased from Harlan and housed at the Erasmus MC facilities. The litters used in this work were born from timed pregnancies, taking the day of birth as P0. Experiments complied with institutional and international guidelines for the use of laboratory animals.

Immunohistochemistry. VGLUT immunohistochemistry was performed as described (ref. 28 and *SI Materials and Methods*).

Multispectral Laser-Scanning Microscopy. Confocal imaging was performed as described (ref. 29 and *SI Materials and Methods*).

Surgery and Tracer Injections. Neonate (P0–3) rat pups were anesthetized with isoflurane (2%, 1 liter of O_2 per min^{-1}), supine-positioned on top of a homeothermic blanket heated to 36–37°C (FHC, Inc.) and secured to a custom-made head holder. After skin retraction, fat and muscle layers overlying the trachea were bluntly removed. Animals were tracheotomized, intubated, and mechanically ventilated using a MiniVent type 845 mouse ventilator (80 breaths per min^{-1}, 60 μl; Hugo-Sachs Elektronik). At this point, anesthesia was reduced to 1.5% and carefully monitored on the basis of pedal reflexes or signs of distress. A small craniotomy (3 $\times$ 2 mm) was drilled above the basilar artery where the anterior inferior cerebellar artery branches, and the dura was opened and retracted. Broken borosilicate glass micropipettes (tip 10–20 μm) were filled with a 10% solution of Alexa Fluor 568–dextran amine tracer (Invitrogen) initially diluted in 0.4 M KCl, but in later experiments in 0.5 M NaCl. Tracer-filled electrodes were positioned next to the basilar artery $\approx$300 $\pm$ 50 μm rostral to the anterior inferior cerebellar artery by using a micromanipulator under visual control. Iontophoretic injections of tracer were delivered at a depth of 100–200 μm with continuous 0.25-s pulses of positive current (0.5 μA) applied through a customized pipette holder at $\approx$2 Hz for 15 s. After tracer injection, the craniotomy was irrigated every 15 min for 1–2 h with 0.9% saline solution until the start of the imaging session. Subsequent histological analysis confirmed that these injections were correctly targeted to the caudal pole of the MNTB (Fig. S2).

Two-Photon Imaging and Analysis. *In vivo* imaging was performed with a custom-built two-photon laser-scanning microscope. Excitation at 800 nm was done with a Ti:sapphire MIRA 900 laser pumped by a 5-W Verdi laser (Coherent, Inc.) coupled into a BX50WI Olympus microscope. Fluorescence was bandpass-filtered (580–680 nm; Semrock) and detected in epifluorescence mode by a cooled PMT (Hamamatsu photosensor module H7422-40). Maximum laser power was $\approx$150 mW, measured after the objective. Image stacks were acquired with a water-immersion objective (Olympus LUMPlanFI, 40$\times$x/0.8 IR) and consisted of 100–150 optical sections (1,024 $\times$ 1,024 pixels; $\approx$0.25-μm per pixel; interval 1–3 μm). Image stacks were imported into Volocity (Improvision), and collaterals were drawn digitally using built-in functions. Axon collaterals $<$2 μm were excluded from the analysis. For each collateral, the length at 1 h was subtracted from its initial length, and these numbers were used to further categorize collaterals in five groups. Criteria for categorizing axon and calyx of Held collaterals are provided in *SI Materials and Methods*.

Slice Electrophysiology and Calcium Imaging. Brain slices were prepared as described in ref. 30, except that rat pups were between P0 and P4 of age. Some experiments also included the application of an anterograde tracer to label afferent axons (28). Whole-cell recordings were performed as described in ref. 30. Details of intracellular solutions and drugs are given in *SI Materials and Methods*. Calyces of Held in brainstem slices containing the MNTB were loaded with the calcium indicator Oregon green BAPTA-1 (OGB-1, 100 μM) via the patch pipette and imaged with two-photon excitation at 800 nm. Four presynaptic action potentials at 10-ms intervals were elicited with depolarizing current injections of 100–300 pA. Line scans along a curved line drawn on the image, passing through one or more collaterals and part of the calyx, were made continuously at 0.125–0.25-μm per pixel at a pixel dwell time of 2 μs. In addition, to correlate morphology and calcium transients, a z-stack was collected.

ACKNOWLEDGMENTS. We thank C. Donkersloot for building and maintaining the two-photon microscope, S. Rusu for ImageJ macros, A. Arredouani for contributing some of the experiments analogous to Fig. S3, and C. Hansel and J. Lorteije for commenting on a previous version of the manuscript. Confocal scanning microscopy was accessed through the Optical Imaging Center at Erasmus MC. This work was supported by FP6 European Union Grant EUsynapse, LSHM-CT-2005–019055, a Neuro-Bsik Grant (Senter, The Netherlands), and equipment grants from the J.H.W. Pasmanstichting and from Netherlands Organization for Scientific Research (911-04-020).

1. McAllister AK (2007) Dynamic aspects of CNS synapse formation. *Annu Rev Neurosci* 30:425–450.
2. Cohen-Cory S, Lom B (2004) Neurotrophic regulation of retinal ganglion cell synaptic connectivity: From axons and dendrites to synapses. *Int J Dev Biol* 48:947–956.
3. Portera-Cailliau C, Weimer RM, De Paola V, Caroni P, Svoboda K (2005) Diverse modes of axon elaboration in the developing neocortex. *PLoS Biol* 3:e272.
4. Javaherian A, Cline HT (2005) Coordinated motor neuron axon growth and neuromuscular synaptogenesis are promoted by CPG15 *in vivo*. *Neuron* 45:505–512.
5. Meyer MP, Smith SJ (2006) Evidence from *in vivo* imaging that synaptogenesis guides the growth and branching of axonal arbors by two distinct mechanisms. *J Neurosci* 26:3604–3614.
6. Ruthazer ES, Li J, Cline HT (2006) Stabilization of axon branch dynamics by synaptic maturation. *J Neurosci* 26:3594–3603.
7. Schneggenburger R, Forsythe ID (2006) The calyx of Held. *Cell Tissue Res* 326:311–337.
8. Kil J, Kageyama GH, Semple MN, Kitzes LM (1995) Development of ventral cochlear nucleus projections to the superior olivary complex in gerbil. *J Comp Neurol* 353:317–340.
9. Kandler K, Friauf E (1993) Pre- and postnatal development of efferent connections of the cochlear nucleus in the rat. *J Comp Neurol* 328:161–184.
10. Hoffpauir BK, Grimes JL, Mathers PH, Spirou GA (2006) Synaptogenesis of the calyx of Held: Rapid onset of function and one-to-one morphological innervation. *J Neurosci* 26:5511–5523.
11. Chuhma N, Ohmori H (1998) Postnatal development of phase-locked high-fidelity synaptic transmission in the medial nucleus of the trapezoid body of the rat. *J Neurosci* 18:512–520.
12. Taschenberger H, Leão RM, Rowland KC, Spirou GA, von Gersdorff H (2002) Optimizing synaptic architecture and efficiency for high-frequency transmission. *Neuron* 36:1127–1143.
13. Wimmer VC, Horstmann H, Groh A, Kuner T (2006) Donut-like topology of synaptic vesicles with a central cluster of mitochondria wrapped into membrane protrusions: A novel structure-function module of the adult calyx of Held. *J Neurosci* 26:109–116.
14. Uziel A, Romand R, Marot M (1981) Development of cochlear potentials in rats. *Audiology* 20:89–100.
15. Morest DK (1968) The growth of synaptic endings in the mammalian brain: A study of the calyces of the trapezoid body. *Zeitschrift Anat Entwicklungs* 127:201–220.
16. Erazo-Fischer E, Striessnig J, Taschenberger H (2007) The role of physiological afferent nerve activity during *in vivo* maturation of the calyx of Held synapse. *J Neurosci* 27:1725–1737.
17. Youssoufian M, Couchman K, Shivdasani MN, Paolini AG, Walmsley B (2008) Maturation of auditory brainstem projections and calyces in the congenitally deaf (*dn/dn*) mouse. *J Comp Neurol* 506:442–451.
18. Bergsman JB, De Camilli P, McCormick DA (2004) Multiple large inputs to principal cells in the mouse medial nucleus of the trapezoid body. *J Neurophysiol* 92:545–552.
19. Futai K, Okada M, Matsuyama K, Takahashi T (2001) High-fidelity transmission acquired via a developmental decrease in NMDA receptor expression at an auditory synapse. *J Neurosci* 21:3342–3349.
20. Morest DK (1968) The collateral system of the medial nucleus of the trapezoid body of the cat, its neuronal architecture, and relation to the olivo-cochlear bundle. *Brain Res* 9:288–2311.
21. Ahmari SE, Buchanan J, Smith SJ (2000) Assembly of presynaptic active zones from cytoplasmic transport packets. *Nat Neurosci* 3:445–451.
22. Shapira M, *et al.* (2003) Unitary assembly of presynaptic active zones from Piccolo–Bassoon transport vesicles. *Neuron* 38:237–252.
23. Alsina B, Vu T, Cohen-Cory S (2001) Visualizing synapse formation in arborizing optic axons *in vivo*: Dynamics and modulation by BDNF. *Nat Neurosci* 4:1093–1101.
24. Hu B, Nikolakopoulou AM, Cohen-Cory S (2005) BDNF stabilizes synapses and maintains the structural complexity of optic axons *in vivo*. *Development* 132:4285–4298.
25. Banks MI, Smith PH (1992) Intracellular recordings from neurobiotin-labeled cells in brain slices of the rat medial nucleus of the trapezoid body. *J Neurosci* 12:2819–2837.
26. Hamann M, Billups B, Forsythe ID (2003) Noncalyceal excitatory inputs mediate low-fidelity synaptic transmission in rat auditory brainstem slices. *Eur J Neurosci* 18:2899–2902.
27. Witte S, Stier H, Cline HT (1996) *In vivo* observations of time course and distribution of morphological dynamics in *Xenopus* retinotectal axon arbors. *J Neurobiol* 31:219–234.
28. Rodriguez-Contreras A, de Lange RP, Lucassen PJ, Borst JGG (2006) Branching of calyceal afferents during postnatal development in the rat auditory brainstem. *J Comp Neurol* 496:214–228.
29. Dickinson M (2005) *Live Cell Imaging, a Laboratory Manual*, eds Goldman RD, Spector DL (Cold Spring Harbor Lab Press, Cold Spring Harbor, NY), pp 281–301.
30. Habets RLP, Borst JGG (2005) Post-tetanic potentiation in the rat calyx of Held synapse. *J Physiol (London)* 564:173–187.